Macromolecules

Article

Cite This: Macromolecules XXXX, XXX, XXX-XXX

pubs.acs.org/Macromolecules

Phase Behavior of Pyrene and Vinyl Polymers with Aromatic Side Groups

Gagan N. Kangovi and Sangwoo Lee*

Department of Chemical and Biological Engineering, Rensselaer Polytechnic Institute, Troy, New York 12180, United States

Supporting Information

ABSTRACT: The phase behavior and thermodynamic properties of mixtures of pyrene and model vinyl polymers with and without aromatic side groups are investigated using differential scanning calorimetry (DSC) measurements. The melting temperature and associated heat of melting of the pyrene crystals in the mixtures are utilized to extract the effective interaction parameters χ and the composition of polymer-rich phases, respectively. The χ of pyrene mixed with polymers with aromatic side groups investigated in this study, polystyrene, poly(2-vinylpyridine), and poly(3-vinylanisole), is less than 0.5 at the melting point of the pyrene crystals, suggesting that pyrene and the polymers with aromatic sides groups are enthalpically compatible, likely due to aromatic $\pi-\pi$ interactions. In contrast, the χ of pyrene mixed with poly(1,4-isoprene) or poly(ethylene-*alt*-propylene) is larger than 0.5. The DSC measurements also enable characterization of the composition of polymer-rich phases. Interestingly, the polymers with aromatic side groups are found to have more pronounced miscibility with pyrene at symmetric compositions.

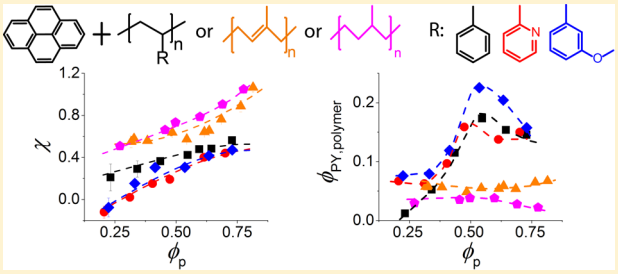

INTRODUCTION

Polycyclic aromatic hydrocarbons (PAHs) are planar organic molecules made of benzene rings with shared ethylene groups.[1] The fused aromatic ring structures delocalize the π-orbital electrons in the PAHs, giving the hydrocarbon molecules high thermal stability[2] and desirable electrical[3] and optical[4] properties for diverse practical applications, including fluorescent dyes and a variety of photonic devices.[5−8] The delocalized π electrons and unique planar structures impart strong self-associations in PAHs, which have also been employed to design and fabricate unique self-assembly materials.[8,9] However, the strong self-preference of PAHs often causes difficulties in incorporating PAHs with other compounds.[10]

Alloying polymers and other functional compounds affords unique opportunities to combine complementary physical and chemical properties of polymers and other components.[11,12] Although the macromolecular character of polymers inherently imposes an entropic penalty in mixing with other compounds,[13] judicious choice of functional groups with favorable enthalpic associations between components has enabled the effective mixing of polymers and other compounds. In this regard, the phase behavior of polymers and solvent has been investigated for practical applications and scientific interest.[14−16] To investigate the experimental phase behaviors of polymer solutions, diverse characterization techniques, for example, cloud point measurements, osmometry, neutron scattering, and light scattering techniques, have been employed.[17] The experimentally observed phase behaviors have been incorporated with thermodynamic state functions, primarily based on the Flory−Huggins theory, to understand the origin of the phase states of the systems of interest.[18,19] In this practice, elucidation of the interaction parameter χ between polymers and solvents has been the central task because χ describes the macroscopic phase states of mixtures and the microscopic states of polymer chains.[20]

In the Flory−Huggins theory, the Gibbs free energy of mixing for a polymer−solvent system per mole of lattice sites is

$$\frac{\Delta G_{mix}}{RT} = \phi_s \ln \phi_s + \frac{\phi_p}{N} \ln \phi_p + \phi_s \phi_p \chi \quad (1)$$

where ϕ_s and ϕ_p are the volume fractions of the solvent and polymer, respectively, and $\phi_s + \phi_p = 1$; N is the number of lattice sites occupied by a polymer chain, which is the degree of polymerization based on the volume of a lattice site; R is the gas constant; and T is the temperature. A solvent molecule is assumed to occupy one lattice site. The first two terms on the right side represent the combinatorial entropy of mixing, $-\Delta S_C/R = \phi_s \ln \phi_s + (\phi_p/N) \ln \phi_p$. The last term, $\phi_s \phi_p \chi RT$, represents the free energy change during mixing due to two contributions: enthalpic interactions between the polymer and solvent and a noncombinatorial entropic term that is not accounted for in ΔS_C. The interaction parameter is often expressed as a function of temperature and composition to describe the enthalpic and noncombinatorial entropic contributions:

$$\chi = A + \frac{B}{T} = A_0 + A_1 \phi_p + \frac{B}{T} \quad (2)$$

Received: September 1, 2017
Revised: October 4, 2017

DOI: 10.1021/acs.macromol.7b01893
Macromolecules XXXX, XXX, XXX−XXX

where $A = A_0 + A_1\phi_p$ represents the noncombinatorial entropic contribution and B represents the enthalpic contribution to the free energy of mixing.[20,21] Thus, the change in the noncombinatorial entropy of the system is $\Delta S_{NC}/RT = -A\phi_s\phi_p$, and the heat of mixing is $\Delta H_{mix}/R = B\phi_s\phi_p$.[20]

The noncombinatorial entropy (ΔS_{NC}) accounts for the entropic contributions to the free energy change during mixing, except for the combinatorial entropy ΔS_C, which involves effects from the orientation of adjacent segments in the polymer chains, the polymer chain conformation, the segment/solvent packing, and the free volume change during mixing.[13,20,22,23] For example, in aqueous solutions of water-soluble polymers, the ordering of water molecules via hydrogen bond formation with polymer chains decreases the entropy of water.[22,24] In contrast, protein folding in water often increases the entropy of solvents due to the reduction in the excluded volume.[25] In addition, polymer swelling in good solvents decreases the entropy of the chains.[13] Since χ contains ΔS_{NC} and ΔH_{mix}, the determination of χ may reveal the thermodynamic characteristics of mixing in the mixtures.

We investigated the phase behavior of binary mixtures of model vinyl polymers and pyrene to quantify the effect of aromatic groups on the thermodynamic properties of polymer and PAH mixtures (Figure 1). The pyrene and polymer

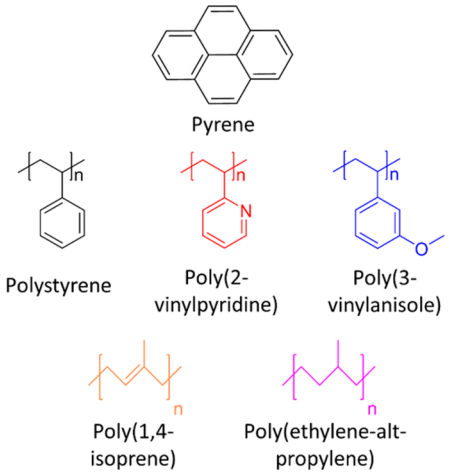

Figure 1. Molecular structures of pyrene and the polymers employed in this study.

mixtures form homogeneous solutions at elevated temperatures but develop two phases, i.e., a polymer-rich phase and a pure pyrene crystal phase, when the mixtures are cooled to below the crystallization temperature of pyrene in the mixtures. Model polymers with different aromatic side groups were chosen to identify the varying degree of miscibility with pyrene.[26] Polystyrene was selected as a reference polymer with neutral aromatic side groups. Poly(2-vinylpyridine) has relatively electron-deficient pyridine side groups due to the electron-withdrawing nitrogen atom in the heterocyclic ring.[27] In contrast, poly(3-vinylanisole) has relatively electron-rich aromatic rings because the methoxy group of anisole is electron donating due to resonance effects.[28] These polystyrene-derivative polymers with a gradient of electron-rich to electron-deficient aromatic rings were chosen to test the effects of the characteristics of delocalized π electrons in the aromatic side groups on the miscibility with pyrene. Polyisoprene and poly(ethylene-*alt*-propylene) were selected as polymers with nonaromatic side groups. Pyrene, one of the smallest PAHs, is composed of four fused benzene rings and is widely utilized as a fluorescent dye and in electronic devices.[5,29] Because of its technological importance and relatively low melting point ($T_{m,PY}$ = 154 °C, see Figure S1), pyrene was selected as the model PAH in this study. Using differential scanning calorimetry (DSC) measurements, we constructed phase portraits of the pyrene and polymer mixtures, extracted the χ's of the model polymers and pyrene, and estimated the chemical composition of the polymer-rich phase in the two-phase states.[20,30] The solubility parameters of pyrene and model polymers from other studies and estimated from the χ's extracted in this study are listed in Table 1 (see below).

Table 1. Solubility Parameters of Pyrene and Model Polymers from Other Studies

compound	solubility parameter ($MPa^{1/2}$)	
	literature[a]	this study[b]
pyrene	23.6 ± 1.7	21.7[c]
polystyrene	18.5 ± 0.4	18.8 ± 0.5
poly(2-vinylpyridine)	21.5 ± 0.4	19.6 ± 1.0
poly(3-vinylanisole)	20.1 ± 0.1	19.1 ± 0.5
poly(1,4-isoprene)	16.5 ± 0.3	17.8 ± 0.4
poly(ethylene-*alt*-propylene)	15.9 ± 0.1	17.6 ± 0.5

[a]Solubility parameters of the model polymers reported in the other studies. The reported parameters are averaged and their standard deviations are noted. The solubility parameters are from the following references: pyrene,[31−34] polystyrene,[35,36] poly(2-vinylpyridine),[37−39] poly(3-vinylanisole),[40,41] polyisoprene,[35,36] and poly(ethylene-*alt*-propylene).[42,43] [b]Solubility parameters extracted from the experimentally determined χ in this study. [c]The solubility parameter of pyrene is assumed to be the 21.7 $MPa^{1/2}$ for extraction of the solubility parameters of polymers.[33]

EXPERIMENTAL SECTION

Materials. Styrene (Acros) and 3-vinylanisole (Aldrich) were purified twice over di-*n*-butylmagnesium and vacuum distilled. 2-Vinylpyridine (Acros) was purified by passing the monomer through activated basic alumina. Isoprene (Acros) was purified over *n*-butyllithium twice and vacuum distilled. The purified monomers were immediately used to synthesize the target polymers. *sec*-Butyllithium (Acros) and pyrene (Alfa Aesar, 98%) were used as received. Tetrahydrofuran (Sigma-Aldrich, HPLC grade) was purified by passing through activated alumina pellets (BASF F-200). Cyclohexane (Sigma-Aldrich, ACS grade) was purified by passing through activated alumina (BASF F-200) and copper catalyst pellets (BASF Q-5). Nickel(II) 2-ethylhexanoate (Aldrich, 0.1 M solution in 2-ethylhexanoic acid) and triethylaluminum (Aldrich, 1 M solution in hexane) were used as received for catalyst preparation for hydrogenation.

Polymerization. All polymers used in this study were prepared by standard high-vacuum anionic polymerization techniques.[44] Polystyrene and polyisoprene were polymerized in cyclohexane at 40 °C.[45] Poly(2-vinylpyridine) and poly(3-vinylanisole) were polymerized in tetrahydrofuran at −78 °C.[46,47] *sec*-Butyllithium was used as the initiator in the synthesis of all polymers. Poly(ethylene-*alt*-propylene) was prepared by the hydrogenation of polyisoprene in cyclohexane at 77 °C and 600 psi for 24 h using a Ni−Al catalyst.[48] Complete hydrogenation of the double bonds of the polyisoprene precursor polymer was confirmed by ^{1}H NMR spectroscopy.

Polymer Characterization. The molecular weight and polydispersity of the synthesized polymers were determined by size exclusion chromatography (SEC, Agilent). Three consecutive PLGel Mixed-C columns were used as the stationary phase, and

DOI: 10.1021/acs.macromol.7b01893
Macromolecules XXXX, XXX, XXX−XXX

tetrahydrofuran (30 °C) or *N*,*N*-dimethylformamide (45 °C) at a flow rate of 1 mL/min was used as the mobile phase. Chromatograms were recorded using a refractive index detector. The chemical composition and molecular weight were determined by ^{1}H NMR spectroscopy (Bruker 800 MHz spectrometer).

Sample Preparation for Calorimetric Measurements. Samples employed for calorimetric characterizations were prepared as follows. Polymer and pyrene solutions in dichloromethane were dried at room temperature. The dried polymer and pyrene mixtures were homogenized at 165 °C for 10 min and then rapidly quenched in liquid nitrogen. This process produced well-dispersed mixtures of pyrene crystals and polymer-rich phases. The homogeneity of the quenched samples was confirmed by the ^{1}H NMR analysis of specimens sampled from different parts of the quenched mixtures.

Calorimetric Measurements. Thermal characterization of the polymer and pyrene mixtures was conducted using DSC (Q2000 TA Instruments) with the following procedure: a sample contained in a hermetic aluminum pan was heated to 200 °C for 20 min, cooled to 85 °C, annealed for 5 h to saturate the pyrene crystal domains, cooled to −50 °C, and heated again. On the final heating, the melting point and associated melting energy of the pyrene crystals in the mixture were determined. The end point of the melting peak was taken as the melting temperature of the pyrene crystals (see Figure S1 for an example). The polyisoprene samples were heated to 170 °C instead of 200 °C to minimize the thermal degradation of polyisoprene.[49]

Wide-Angle X-ray Scattering. Wide-angle X-ray scattering (WAXS) experiments were conducted at the 11-BM, 12-ID-B, and 5-ID beamlines at the Advanced Photon Source at Argonne National Laboratory. Mixtures of pyrene and polymers contained in sealed ampules were heated and homogenized at 165 °C, annealed at 85 °C for at least 5 h, and quenched to room temperature. The polymer and pyrene mixtures were powdered using an agate mortar and pestle and contained quartz (Charles-Supper) or Kapton capillaries for the X-ray scattering experiments. The unit cell parameters of the pyrene crystals were extracted using the "FOX" software[50] and the Rietveld powder pattern simulation function of the X'Pert High Score software (PANalytical).

RESULTS AND DISCUSSION

Table 2 lists the molecular characterization data of the polymers employed in this study. All polymers have number-averaged molecular weights from 16 to 25 kg/mol, and their molecular weight distributions are monomodal with polydispersity $Đ < 1.15$.

Table 2. Polymer Characterization Data

polymer	M_n[a] (kg/mol)	$Đ$[b]	ρ[c] (g/cm^3)	N[d]
polystyrene	23.4[e]	1.13	1.04	159
poly(2-vinylpyridine)	20.3[f]	1.02	1.12	166
poly(3-vinylanisole)	16.1[f]	1.10	1.10	110
polyisoprene	24.6[g]	1.07	0.91	180
poly(ethylene-*alt*-propylene)	25.5[h]	1.09	0.856	187

[a]Number-averaged molecular weight. [b]The polydispersity indices were determined by SEC. [c]Density at 25 °C.[36,51−53] [d]Degree of polymerization based on the molar volume of crystalline pyrene (159 cm^3/mol).[54] [e]The molecular weight of polystyrene was determined by SEC using polystyrene standards. [f]The molecular weights of poly(2-vinylpyridine) and poly(3-vinylanisole) were determined by end-group analysis of their ^{1}H NMR spectra. [g]The molecular weight of polyisoprene was determined by the Mark−Houwink parameters (a = 0.731 and k = 15.7 × 10^{-5} dL/g).[55] Polyisoprene is composed of 94% 1,4-configuration and 6% 3,4-configuration. [h]The molecular weight of poly(ethylene-*alt*-propylene) was determined by stoichiometric calculations based on 100% hydrogenation (confirmed by ^{1}H NMR) of poly(1,4-isoprene) with a molecular weight of 24.8 kg/mol.

Figure 2 shows the DSC thermograms obtained from the final heating of the polymer and pyrene mixtures, which were cooled to 85 °C, annealed at 85 °C for 5 h, and cooled to −50 °C before the final heating. The annealing temperature of 85 °C was chosen because it is higher than the glass transition temperatures of the mixtures (down arrows in Figure 2) and low enough to induce pyrene crystallization in all the mixtures. In the heating curves, polymer mixtures containing more than 20 wt % pyrene showed endothermic peaks for the melting of pyrene crystals. The end points of the melting peaks were taken as the melting temperatures of the pyrene crystals and the binodal points between the single-phase mixtures and the two phase states of pyrene crystal and polymer solution. To identify binodal points by thermal scanning, material systems can be cooled or heated to detect phase separation or the mixing of phase-separated domains, but nucleation barriers can be encountered in both directions, which makes the precise identification of binodal points difficult. However, the homogenization of phase-separated states is known to experience weaker nucleation barriers because grain boundaries and domain surfaces act as nucleates for the fast initiation of homogenization processes.[56] Thus, we considered the melting temperatures of the pyrene crystals to be the binodal points of the polymer and pyrene mixtures. The melting temperatures were determined by DSC measurements at least three times to confirm the reproducibility. The melting temperatures of the pyrene crystals were found to be consistent within ±1 °C at different heating rates. The heating rate of 10 °C/min was chosen to quantify the energy associated with the melting of the pyrene crystals. In all mixtures, the melting temperature of the pyrene crystals increased as the weight fraction of pyrene in the mixture increased.

The one-dimensional X-ray scattering patterns obtained from selected polymer and pyrene mixtures showed Bragg peaks (Figure S2), but the relative intensities of the Bragg peaks varied between samples due to the large grain size of the pyrene crystals, as indicated by the strong Bragg spots on the two-dimensional X-ray scattering patterns in Figure S3. Indexing by the ab initio method and Rietveld powder pattern simulations confirmed that the Bragg peaks represent a monoclinic crystal symmetry $P2_1/a$ (space group no. 14) with lattice parameters a = 13.5 Å, b = 9.16 Å, c = 8.36 Å, and β = 100.4°, which is consistent with the known symmetry and lattice parameters of pyrene crystals at ambient pressure and temperature (Figure S4).[57,58] The scattering patterns obtained from the polymer and pyrene mixtures at 175 °C > $T_{m,PY}$ show a broad featureless peak, which confirms that the pyrene molecules are in the molten state (Figure S5).

Figure 3 presents the phase portrait of the pyrene and polymer mixtures, and Table 3 summarizes the melting temperature and the associated exothermic energy of the pyrene crystals, obtained from the DSC thermograms in Figure 2. The melting temperatures of the pyrene crystals in mixtures with the same composition decrease in the order of poly(ethylene-*alt*-propylene), polyisoprene, polystyrene, poly(3-vinylanisole), and poly(2-vinylpyridine) (Figure 3 and Table 3). We extracted the effective interaction parameters (χ) of the polymer and pyrene mixtures using the melting temperature of the pyrene crystals.[13,20,30] As pyrene crystals in a mixture melt, two thermodynamic events occur: solid pyrene crystals become liquid, and the liquid pyrene molecules mix with the polymer chains. The chemical potential involved in the melting of pyrene crystals to a pure liquid state is

DOI: 10.1021/acs.macromol.7b01893
Macromolecules XXXX, XXX, XXX−XXX

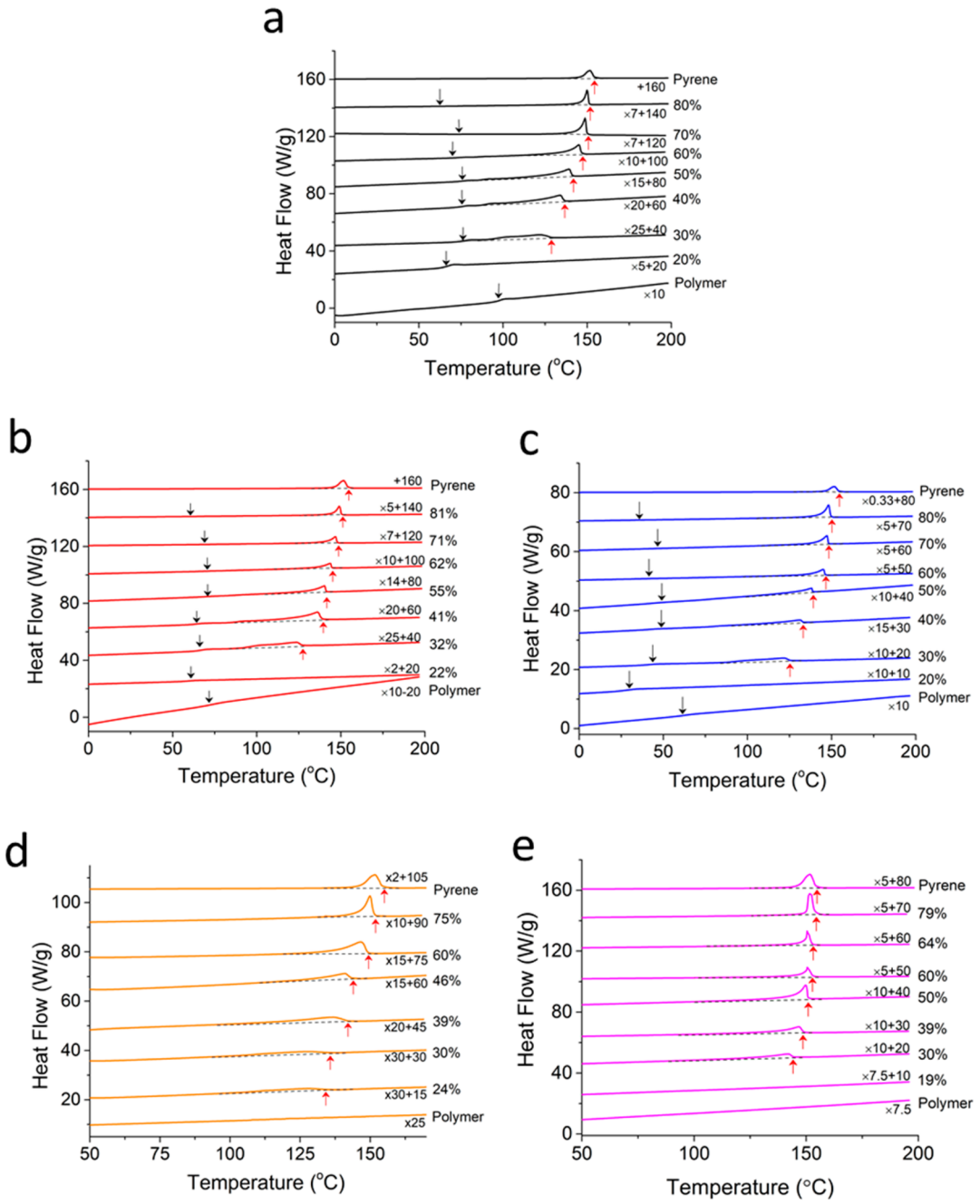

Figure 2. DSC thermograms of mixtures of pyrene and (a) polystyrene, (b) poly(2-vinylpyridine), (c) poly(3-vinylanisole), (d) polyisoprene, and (e) poly(ethylene-*alt*-propylene). The heat flows are represented in the "endo-up" form. The red arrows indicate the melting temperatures of the pyrene crystals, and the black arrows indicate the glass transition temperatures. The weight percent of pyrene in the mixtures and the magnification factors are noted next to the thermograms. The thermograms are shifted for clearer representation. The shift factor is given at the bottom right of each thermogram.

$$\mu_{l,PY} - \mu_{c,PY} = (\Delta H_{m,PY(mix)} - T_m \Delta S_{m,PY(mix)}) = \Delta H_{m,PY}\left(1 - \frac{T_m}{T_{m,PY}}\right) \quad (3)$$

where $\mu_{l,PY}$ and $\mu_{c,PY}$ are the chemical potentials of pure liquid pyrene and crystalline pyrene, respectively; $\Delta H_{m,PY(mix)}$ and $\Delta S_{m,PY(mix)}$ are the changes in enthalpy and entropy, respectively, associated with pyrene melting; and T_m is the melting temperature of pyrene crystals in a mixture. In eq 3, $\Delta S_{m,PY(mix)}/\Delta H_{m,PY(mix)}$ is assumed to be independent of the melting temperature of the pyrene crystals, and $\Delta S_{m,PY(mix)}/\Delta H_{m,PY(mix)} = \Delta S_{m,PY}/\Delta H_{m,PY} = 1/T_{m,PY}$, where $\Delta H_{m,PY}$ and $\Delta S_{m,PY}$ are the enthalpy and entropy of pure pyrene at the melting temperature of pure pyrene crystals, $T_{m,PY}$.[30] Thus, the difference in the chemical potentials becomes a function of T_m on the right side of eq 3. $\Delta H_{m,PY} = 86$ J/g and $\Delta H_{m,PY} = 427$ K were experimentally determined from the DSC characterization of pure pyrene crystals, and these quantities are consistent with the values reported elsewhere (Figure S1).[54] The change in the chemical potential involved in the mixing of liquid pyrene and polymer is

DOI: 10.1021/acs.macromol.7b01893
Macromolecules XXXX, XXX, XXX−XXX

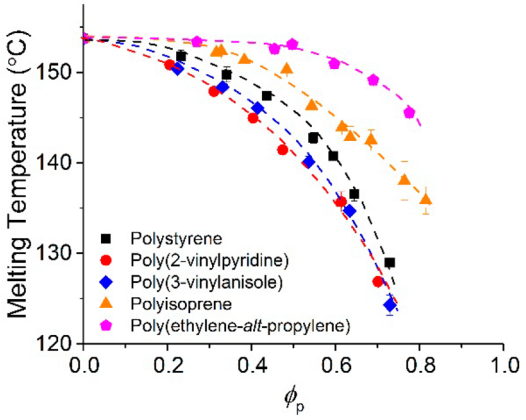

Figure 3. Phase portraits of binary mixtures of pyrene and model polymers.

$$\mu_{l,PY(mix)} - \mu_{l,PY} = \left[\ln(1-\phi_p) + \left(1-\frac{1}{N}\right)\phi_p + \chi\phi_p^2\right]RT \quad (4)$$

where $\mu_{l,PY(mix)}$ is the chemical potential of pyrene in a polymer and pyrene solution.[20] As pyrene crystals in a polymer mixture melt, the chemical potentials of pyrene molecules in their crystalline and mixed states are identical, i.e., $\mu_{l,PY(mix)} = \mu_{c,PY}$. Thus, combining eqs 3 and 4 gives

$$\frac{1}{T_m} - \frac{1}{T_{m,PY}} = -\frac{R}{\Delta H_{m,PY}}\left[\ln(1-\phi_p) + \left(1-\frac{1}{N}\right)\phi_p + \chi\phi_p^2\right] \quad (5)$$

Equation 5 extracts the effective interaction parameter χ between pyrene and the polymer at a given composition using the melting temperature of pyrene crystals in the polymer mixture.

The extracted χ's from the polymer and pyrene mixtures are presented in Figure 4. The χ's between pyrene and the polymers without aromatic groups, i.e., polyisoprene and poly(ethylene-*alt*-propylene), are larger than the critical interaction parameter of miscibility, $\chi_c = 0.5(1/N + 2/N^{1/2} + 1) \approx 0.58$. In contrast, the effective interaction parameters between pyrene and the polymers with aromatic side groups, $\chi_{PAr} < 0.5$, indicate that these polymers are more miscible with pyrene than polyisoprene or poly(ethylene-*alt*-propylene). Although the χ's between pyrene and the polymers without aromatic side groups are higher than the critical interaction parameter, the mixtures did not show any sign of liquid−liquid phase separation at temperatures higher than the melting point of the pyrene crystals.

The interaction parameter constants based on eq 2 are summarized in Table 4. The Flory−Huggins theory defines the interaction parameter to be linearly proportional to the inverse temperature T^{-1}.[13] However, the effective interaction parameters for the mixtures of pyrene and polymers with aromatic side groups (χ_{PAr}) exhibit nonlinear increases with T^{-1} (Figure 4). Rather, χ_{PAr} is linearly proportional to the polymer volume fraction up to $\phi_p = 0.6$. The linear dependence of χ_{PAr} suggests that the microscopic states of mixing between pyrene and the polymer segments vary depending on the mixture composition, and significant noncombinatorial entropy contributions are present in the mixing of pyrene and polymers with aromatic side groups.[59] The effective interaction parameters of polyisoprene (χ_{PI}) and poly(ethylene-*alt*-propylene) (χ_{PEP}) also increase with T^{-1} and ϕ_p over the entire temperature and composition range investigated, and χ_{PI} and χ_{PEP} also increase linearly with ϕ_p. χ_{PAr} is asymptotic at high T^{-1} and ϕ_p, but χ_{PI} and χ_{PEP} are divergent. These differences in the characteristics of χ indicate a qualitative difference in the interaction between pyrene and polymers with and without aromatic side groups. However, the steady increase in χ between pyrene and all model polymers with T^{-1} suggests that these binary pairs are upper critical solution temperature (UCST) systems, as shown in Figure 3.[60]

All the interaction parameters between pyrene and the polymers with aromatic side groups (χ_{PAr}) are less than 0.5, and the enthalpic contribution to $\chi_{PAr}(B)$ is negative. Thus, the polymers with aromatic side groups appear to be enthalpically compatible with pyrene, perhaps due to the aromatic ($\pi-\pi$) interactions.[26,61] However, the noncombinatorial entropic contribution to $\chi_{PAr}(A)$ is positive, and thus, an entropic penalty occurs during mixing, likely due to (i) an increase in the polymer chain dimensions[13] and (ii) the restructuring of pyrene molecules around the polymer segments, leading to an increase in the degree of order and a decrease in the free volume of pyrene, which are also observed in polymer solutions with solvents that interact favorably with the polymers.[22,24] The degree of the melting temperature depression and the interaction parameter suggests that poly(2-vinylpyridine) is the most enthalpically compatible with pyrene among the polymers with aromatic side groups investigated in this study,

Table 3. Melting Temperature and Associated Energy Change Characterized by DSC

polystyrene			poly(2-vinylpyridine)			poly(3-vinylanisole)			polyisoprene			poly(ethylene-*alt*-propylene)		
ϕ_p[a]	T_m (°C)	ΔE[b] (J/g)	ϕ_p[a]	T_m (°C)	ΔE[b] (J/g)	ϕ_p[a]	T_m (°C)	ΔE[b] (J/g)	ϕ_p[a]	T_m (°C)	ΔE[b] (J/g)	ϕ_p[a]	T_m (°C)	ΔE[b] (J/g)
0.23	152	65	0.21	151	62	0.22	150	60	0.32	152	56	0.27	146	66
0.34	150	53	0.31	148	53	0.33	148	51	0.33	152	55	0.46	150	49
0.44	147	40	0.40	145	42	0.41	146	40	0.38	151	51	0.50	151	45
0.55	143	25	0.48	141	31	0.54	140	22	0.48	150	43	0.60	153	37
0.65	137	18	0.61	136	22	0.63	135	15	0.54	146	37	0.69	153	29
0.73	129	11	0.70	127	13	0.73	124	10	0.61	144	31	0.78	153	21
									0.63	143	29			
									0.68	143	24			
									0.76	138	16			
									0.81	136	10			

[a]Volume fraction of the polymer. [b]Energy change per gram of binary mixture.

DOI: 10.1021/acs.macromol.7b01893
Macromolecules XXXX, XXX, XXX−XXX

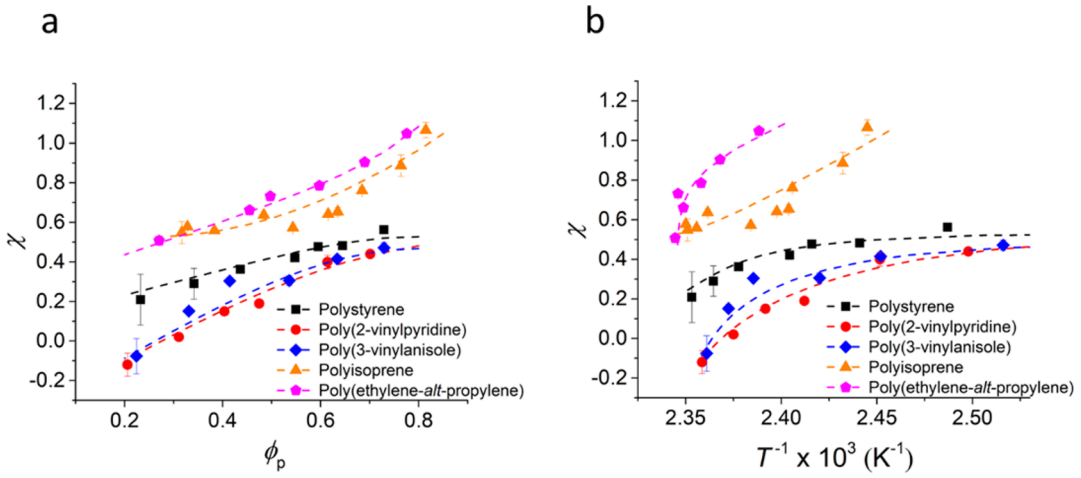

Figure 4. Effective interaction parameters (χ) between pyrene and model polymers depending on (a) the volume fraction of the polymer ϕ_p and (b) the inverse melting temperature of pyrene T^{-1}. The dashed lines represent the interaction parameter functions from eq 2.

Table 4. Constants for the Effective Interaction Parameters of Polymer and Pyrene Mixtures Based on Eq 2, $\chi = A_0 + A_1\phi_p + B/T$

polymer	A_0	A_1	Range of A^a	B (K)
polystyrene	1.3	0.7	1.3 to 2.0	−527
poly(2-vinylpyridine)	4.0	1.6	4.0 to 5.6	−1872
poly(3-vinylanisole)	3.7	1.6	3.7 to 5.3	−1750
polyisoprene	−15.6	−0.4	−16.0 to −15.6	6922
poly(ethylene-*alt*-propylene)	−6.0	0.8	−6.0 to −5.2	2665

$^a A = A_0 + A_1\phi_p$, where $0 < \phi_p < 1$.

and polystyrene is the least compatible (Figure 4). The magnitudes of the B parameters in Table 4 are also consistent with the order of melting point depressions and the magnitude of the dipole moments of the aromatic side groups. The dipole moment of pyridine is 2.2 D, and that of anisole is 1.26 D.[62,63] Benzene, the side group of polystyrene, has zero dipole moment due to its symmetry. This trend suggests that the degree of miscibility between aromatic functional groups is likely due to the strength of the dipole moments of molecular motifs rather than the characteristics of delocalized π electrons in the aromatic groups.

We extracted the solubility parameters of polymers using the interaction parameters determined by the melting temperatures of pyrene crystals using the following relationship:[13]

$$\chi = \frac{V_{m,PY}}{RT}(\delta_{PY} - \delta_p)^2 \quad (6)$$

where $V_{m,PY}$ = 159 cm^3/mol, which is the molar volume of pyrene in its crystalline form;[54] and δ_{PY} and δ_p are the solubility parameters of pyrene and the polymer, respectively. In the extraction of the solubility parameters of polymers, the solubility parameter of pyrene is assumed to be 21.7 $MPa^{1/2}$.[33] Table 1 lists the extracted δ_p values, and the solubility parameters reasonably agree with the values reported in other studies.

Figure 5 shows the ratio between noncombinatorial entropy and enthalpy contributions $A/(B/T)$ in the interaction parameters as a function of ϕ_p and T^{-1}. For mixtures of pyrene and the polymers with aromatic side groups, $A/(B/T)$ increases linearly up to $\phi_p \approx 0.6$ (Figure 5a). Considering that χ represents thermodynamic contributions from noncombina-

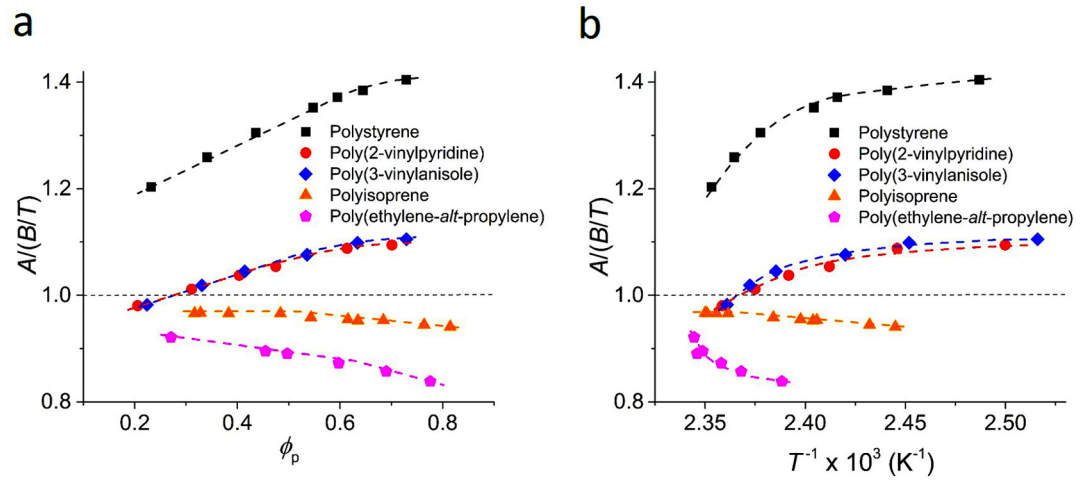

Figure 5. Ratio between noncombinatorial entropy and enthalpy contributions in the interaction parameters as a function of (a) polymer volume fraction ϕ_p and (b) inverse temperature (T^{-1}). The dashed lines are to guide the eye.

DOI: 10.1021/acs.macromol.7b01893
Macromolecules XXXX, XXX, XXX−XXX

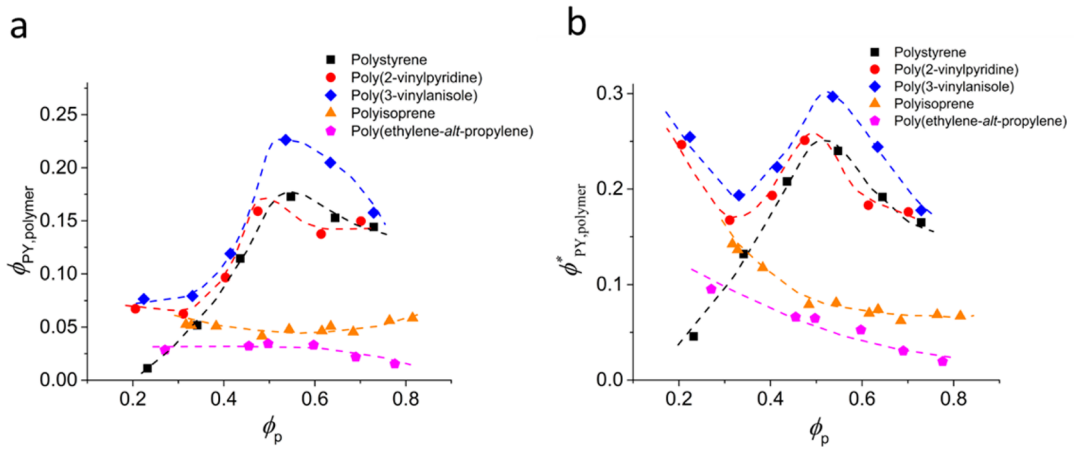

Figure 6. Pyrene compositions in the two-phase states at 85 °C based on the heat of melting of the pyrene crystal. (a) Volume fractions of pyrene dissolved in the polymer-rich phase relative to the total volume of the mixture $\phi_{PY,polymer}$. (b) Volume fraction of pyrene in the polymer-rich phase $\phi^*_{PY,polymer}$.

torial entropy and enthalpy per lattice site, the increasing $A/(B/T)$ of χ_{PAr} indicates that the noncombinatorial entropy penalty of mixing increases as the amount of polymer increases in the mixtures. This suggests that this entropic penalty originates primarily from polymer chain swelling and the limited freedom of polymer segmental motions due to interactions between pyrene and the polymer chains. The asymptotic behavior of the $A/(B/T)$ of χ_{PAr} at $\phi_p > 0.6$ also supports this interpretation because the degree of pyrene and polymer interactions saturates and diminishes as the polymer volume fraction increases.

The negative A parameters in χ_{PI} and χ_{PEP} indicate that noncombinatorial entropy promotes mixing of the polymer and pyrene (Table 4), but the large enthalpic penalty, as indicated by the relatively small $A/(B/T)$ ratios, makes polyisoprene and poly(ethylene-*alt*-propylene) largely incompatible with pyrene.

The most remarkable advantage of using the DSC for the characterization of the thermodynamic properties of mixtures containing a crystallizable component is that the compositions of noncrystalline phases can be extracted from the endothermic heat by melting of the crystals. The DSC thermograms of the polymer and pyrene mixtures annealed at 85 °C are shown in Figure 2, and thus, the amount of pyrene crystals indicated by the endothermic peaks practically represents the phase state of the polymer and pyrene mixtures at this annealing temperature. This reasoning is supported by the observation that the endothermic peaks of the mixtures with low pyrene contents (30−40 wt %) start at approximately 85 °C (Figure 2). The relatively broad melting peaks in these low-pyrene-content mixtures are likely due to the broad size distribution of pyrene crystal grains, and the melting points are lowered due to the interfacial tension between the pyrene crystals and the polymer-rich phase.[64] This reasoning is also qualitatively supported by the 2D WAXS patterns of the polymer and pyrene mixtures (Figure S3). The 2D WAXS patterns obtained from the mixtures containing 30 wt % pyrene present patterns similar to those of powder samples, indicating that the pyrene crystallites are relatively small compared to the pyrene crystals in the 70 wt % pyrene sample. The latter sample produced the WAXS patterns with relatively smaller number of Bragg spots, but the intensities of Bragg spots are much stronger due to larger pyrene crystallites.

We utilized the energy associated with the pyrene melting peaks to quantify the composition of the polymer-rich phase that coexists with the pure pyrene crystals. The endotherm energy (ΔE in Table 3) is the energy per gram of mixtures by (i) the enthalpy of melting of pyrene crystals in the mixture ($\Delta H_{m,PY(mix)}$) and (ii) the energy of mixing of the molten pyrene and polymer. The energy of mixing can be calculated using the ΔG_{mix} defined by eq 1. Since ΔG_{mix} by eq 1 is per mole of lattice sites, the energy of mixing per mass of polymer and pyrene mixture is $\Delta G_{mix}/M_{PY}$ where M_{PY} = 202.25 g/mol is the molar mass of pyrene since the lattice site in this study is assumed for a pyrene molecule. The energy of mixing is the change of $\Delta G_{mix}/M_{PY}$ from 85 °C to T_m. The energy of mixing at 85 °C is $(1 - w_{PY}f_c)\Delta G_{mix}(85\ °C)/M_{PY}$, where w_{PY} is the weight fraction of pyrene and f_c is the pyrene crystallinity in the mixture. The $w_{PY}f_c$ term represent the amount of pyrene crystals, which does not contribute to the energy of mixing. Also, the $\Delta G_{mix}(85\ °C)$ should be evaluated based on the composition of the polymer-rich phase (see below). The energy of mixing $\Delta G_{mix}/M_{PY}$ at T_m is evaluated by the overall composition of mixture. Thus

$$\Delta E = \Delta H_{m,PY(mix)} + \frac{\Delta G_{mix}(T_m) - (1 - w_{PY}f_c)\Delta G_{mix}(85\ °C)}{M_{PY}} \quad (7)$$

Equation 7 extracts $\Delta H_{m,PY(mix)}$, which is used to calculate the crystallinity of pyrene in the mixture $f_c = \Delta H_{m,PY(mix)}/(w_{PY}\Delta H_{m,PY})$ where $\Delta H_{m,PY}$ = 86 J/g. The volume fraction of pyrene in the polymer-rich phase relative to the total volume of the mixture is calculated based on that the coexisting crystalline phases are pure pyrene:

$$\phi_{PY,polymer} = (1 - f_c)(1 - \phi_p) \quad (8)$$

f_c can also be used to determine the volume fraction of molten pyrene relative to the volume of the polymer-rich phase:

$$\phi^*_{PY,polymer} = \frac{(1 - f_c)(1 - \phi_p)}{1 - (1 - \phi_p)f_c} \quad (9)$$

As noted above, the $\Delta G_{mix}(85\ °C)$ should be calculated with $\phi^*_{PY,polymer}$ and the volume fraction of polymer in the polymer-rich phase $\phi^*_p = 1 - \phi^*_{PY,polymer}$. Equations 7−9 are combined, and $\phi_{PY,polymer}$ and $\phi^*_{PY,polymer}$ are numerically determined.

DOI: 10.1021/acs.macromol.7b01893
Macromolecules XXXX, XXX, XXX−XXX

The extracted $\phi_{PY,polymer}$ shows a clear difference depending on the class of polymer, i.e., with or without aromatic side groups (Figure 6a). The polymers with aromatic side groups have more pronounced solubility of pyrene in the polymer phase at symmetric mixture compositions as indicated by $\phi_{PY,polymer}$. The amount of favorable enthalpic interactions between pyrene and the polymers with aromatic side groups are maximized at symmetric compositions. This enhanced miscibility is also clearly observed in the plot of $\phi^*_{PY,polymer}$ (Figure 6b). In contrast, the $\phi^*_{PY,polymer}$ of polyisoprene and poly(ethylene-*alt*-propylene) monotonically decreases with ϕ_p and are smaller than those of the polymers with aromatic side groups, which is consistent with the nonassociating interactions between pyrene and polyisoprene and poly(ethylene-*alt*-propylene).

Figure 7 summarizes the ratio of pyrene in crystalline and molten states denoted by K. The steep decrease of K of the mixtures of pyrene and polymers with aromatic side groups over ϕ_p is also attributed to the favorable interactions between pyrene and the polymers because more polymer in the system means more sites for favorable interactions. In contrast, the K of the poly(1,4-isoprene) and poly(ethylene-*alt*-propylene) mixtures are relatively invariant over ϕ_p due to the large enthalpic incompatibility of these polymers with pyrene.

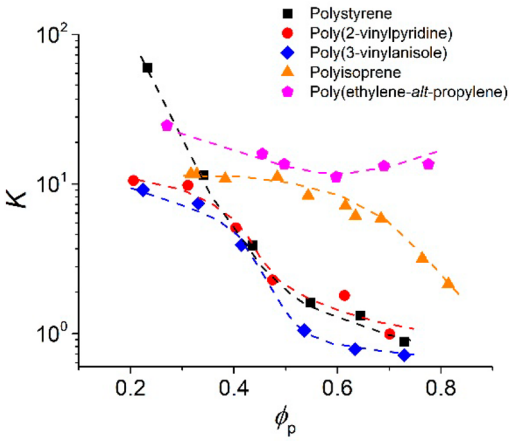

Figure 7. Ratios of pyrene in the crystalline and polymer-rich phases; K = mass of crystalline pyrene/mass of pyrene in the polymer phase. The dashed lines are to guide the eye.

SUMMARY AND CONCLUSIONS

We investigated the phase behaviors of mixtures of pyrene and model polymers with and without aromatic side groups using DSC measurements. The pyrene and polymer mixtures showed two-phase systems consisting of a polymer-rich phase and a pure pyrene crystal phase. Using the Flory–Huggins theory, we extracted the effective interaction parameters between pyrene and the model polymers. The interaction parameters between pyrene and the polymers with aromatic side groups were smaller than 0.5 and had favorable enthalpic interactions for mixing likely due to the π–π interactions between the aromatic groups. In contrast, the interaction parameters between pyrene and poly(1,4-isoprene) or poly(ethylene-*alt*-propylene) are larger than 0.5, though these mixtures formed homogeneous solutions at elevated temperatures upon the melting of pyrene. The DSC characterizations also enabled to measure the composition of the polymer-rich phases. Remarkably, the polymers with aromatic side groups had enhanced miscibility with pyrene at symmetric compositions, likely due to the maximization of enthalpically favorable interactions. This study demonstrates that the DSC technique can be effectively utilized to characterize and measure the phase behavior, thermodynamic properties, and compositions of mixtures with a crystallizable component. The thermodynamic information regarding pyrene and the model polymers gained from this study will be useful for the rational design of polymeric materials incorporating PAHs to obtain target properties and material states;[65,66] for example, tuning the state of asphaltenes with large PAH motifs in crude oils may be achieved using judiciously designed polymeric materials.[67]

ASSOCIATED CONTENT

Supporting Information

The Supporting Information is available free of charge on the ACS Publications website at DOI: 10.1021/acs.macromol.7b01893.

Figures S1–S5 (PDF)

AUTHOR INFORMATION

Corresponding Author

*E-mail: lees27@rpi.edu (S.L.).

ORCID

Sangwoo Lee: 0000-0003-4215-0317

Notes

The authors declare no competing financial interest.

ACKNOWLEDGMENTS

Acknowledgment is made to the donors of the American Chemical Society Petroleum Research Fund for partial support of this research. G.N.K. thanks Ishan Chadha for the assistance of hydrogenation and DSC characterizations. The X-ray scattering characterizations were performed at the 11-BM, 12-ID-B, and 5-ID beamlines at the Advanced Photon Source (APS), partly supported by the U.S. Department of Energy, Office of Science, Office of Basic Energy Sciences, under Contract DE-AC02-06CH11357. The 5-ID line is operated by the DuPont–Northwestern–Dow Collaborative Access Team (DND-CAT) and is also partly supported by Northwestern University, E.I. DuPont de Nemours & Co., and The Dow Chemical Company. Part of the scattering data were collected using an instrument funded by the National Science Foundation under Award 0960140.

REFERENCES

(1) Bandeira, G. C. *Chemistry Research and Applications: Handbook of Polycyclic Aromatic Hydrocarbons: Chemistry, Occurrence and Health Issues*; Nova Science Publishers, Inc.: New York, 2012.

(2) Stein, S. E. Thermal Reactions and Properties of Polycyclic Aromatic Hydrocarbons. *Acc. Chem. Res.* **1991**, *24* (11), 350–356.

(3) Fujii, S.; Enoki, T. Nanographene and Graphene Edges: Electronic Structure and Nanofabrication. *Acc. Chem. Res.* **2013**, *46* (10), 2202–2210.

(4) Fleming, A. J.; Coleman, J. N.; Dalton, A. B.; Fechtenkötter, A.; Watson, M. D.; Müllen, K.; Byrne, H. J.; Blau, W. J. Optical Spectroscopy of Isolated and Aggregate Hexabenzocoronene Derivatives: A Study of Self-Assembling Molecular Nanowires. *J. Phys. Chem. B* **2003**, *107* (1), 37–43.

(5) Winnik, F. M. Photophysics of preassociated pyrenes in aqueous polymer solutions and in other organized media. *Chem. Rev.* **1993**, *93* (2), 587–614.

DOI: 10.1021/acs.macromol.7b01893
Macromolecules XXXX, XXX, XXX–XXX

(6) Bin, J.-K.; Hong, J.-I. Efficient blue organic light-emitting diode using anthracene-derived emitters based on polycyclic aromatic hydrocarbons. *Org. Electron.* **2011**, *12* (5), 802−808.
(7) Wang, X.; Zhi, L.; Tsao, N.; Tomović, Ž.; Li, J.; Müllen, K. Transparent carbon films as electrodes in organic solar cells. *Angew. Chem., Int. Ed.* **2008**, *47* (16), 2990−2992.
(8) Lee, O. P.; Yiu, A. T.; Beaujuge, P. M.; Woo, C. H.; Holcombe, T. W.; Millstone, J. E.; Douglas, J. D.; Chen, M. S.; Fréchet, J. M. Efficient Small Molecule Bulk Heterojunction Solar Cells with High Fill Factors via Pyrene-Directed Molecular Self-Assembly. *Adv. Mater.* **2011**, *23* (45), 5359−5363.
(9) Elemans, J. A.; van Hameren, R.; Nolte, R. J.; Rowan, A. E. Molecular Materials by Self-Assembly of Porphyrins, Phthalocyanines, and Perylenes. *Adv. Mater.* **2006**, *18* (10), 1251−1266.
(10) Hughes, J. M.; Hernandez, Y.; Aherne, D.; Doessel, L.; Müllen, K.; Moreton, B.; White, T. W.; Partridge, C.; Costantini, G.; Shmeliov, A.; Shannon, M.; Nicolosi, V.; Coleman, J. N. High Quality Dispersions of Hexabenzocoronene in Organic Solvents. *J. Am. Chem. Soc.* **2012**, *134* (29), 12168−12179.
(11) Rodríguez-Delgado, M. M.; Alemán-Nava, G. S.; Rodríguez-Delgado, J. M.; Dieck-Assad, G.; Martínez-Chapa, S. O.; Barceló, D.; Parra, R. Laccase-based biosensors for detection of phenolic compounds. *TrAC, Trends Anal. Chem.* **2015**, *74*, 21−45.
(12) Pillai, O.; Panchagnula, R. Polymers in drug delivery. *Curr. Opin. Chem. Biol.* **2001**, *5* (4), 447−451.
(13) Hiemenz, P. C.; Lodge, T. P. *Polymer Chemistry*, 2nd ed.; CRC Press: Boca Raton, FL, 2007.
(14) Dormidontova, E. E. Role of competitive PEO−water and water−water hydrogen bonding in aqueous solution PEO behavior. *Macromolecules* **2002**, *35* (3), 987−1001.
(15) Malcolm, G.; Rowlinson, J. The thermodynamic properties of aqueous solutions of polyethylene glycol, polypropylene glycol and dioxane. *Trans. Faraday Soc.* **1957**, *53*, 921−931.
(16) Oster, G. Dye binding to high polymers. *J. Polym. Sci.* **1955**, *16* (82), 235−244.
(17) Teraoka, I. *Polymer Solutions: An Introduction to Physical Properties*; Wiley: New York, 2002.
(18) Flory, P. J. Fifteenth Spiers Memorial Lecture. Thermodynamics of polymer solutions. *Discuss. Faraday Soc.* **1970**, *49*, 7−29.
(19) Muthukumar, M. Thermodynamics of polymer solutions. *J. Chem. Phys.* **1986**, *85* (8), 4722−4728.
(20) Flory, P. J. *Principles of Polymer Chemistry*; Cornell University Press: Ithaca, NY, 1953.
(21) Freed, K. F.; Pesci, A. I. Theory of the molecular origins of the entropic portion of the Flory χ parameter for polymer blends. *J. Chem. Phys.* **1987**, *87* (12), 7342.
(22) Patterson, D. Free Volume and Polymer Solubility. A Qualitative View. *Macromolecules* **1969**, *2* (6), 672−677.
(23) Fredrickson, G. H.; Liu, A. J.; Bates, F. S. Entropic corrections to the Flory-Huggins theory of polymer blends: Architectural and conformational effects. *Macromolecules* **1994**, *27* (9), 2503−2511.
(24) Bae, Y. H.; Okano, T.; Kim, S. W. Temperature dependence of swelling of crosslinked poly (N, N′-alkyl substituted acrylamides) in water. *J. Polym. Sci., Part B: Polym. Phys.* **1990**, *28* (6), 923−936.
(25) Harano, Y.; Kinoshita, M. Translational-entropy gain of solvent upon protein folding. *Biophys. J.* **2005**, *89* (4), 2701−2710.
(26) Waters, M. L. Aromatic interactions in model systems. *Curr. Opin. Chem. Biol.* **2002**, *6* (6), 736−741.
(27) O'Hara, F.; Blackmond, D. G.; Baran, P. S. Radical-Based Regioselective C−H Functionalization of Electron-Deficient Heteroarenes: Scope, Tunability, and Predictability. *J. Am. Chem. Soc.* **2013**, *135* (32), 12122−12134.
(28) Agrawal, A. K.; Jenekhe, S. A. Synthesis and processing of heterocyclic polymers as electronic, optoelectronic, and nonlinear optical materials. 3. New conjugated polyquinolines with electron-donor or-acceptor side groups. *Chem. Mater.* **1993**, *5* (5), 633−640.
(29) Figueira-Duarte, T. M.; Müllen, K. Pyrene-based materials for organic electronics. *Chem. Rev.* **2011**, *111* (11), 7260−7314.
(30) Nishi, T.; Wang, T. T. Melting Point Depression and Kinetic Effects of Cooling on Crystallization in Poly(vinylidene fluoride)-Poly(methyl methacrylate) Mixtures. *Macromolecules* **1975**, *8* (6), 909−915.
(31) Nikooyeh, K. Phase behavior of asphaltenes in organic media. Ph.D. Dissertation, University of Alberta, Edmonton, 2012.
(32) Hanshaw, W.; Nutt, M.; Chickos, J. S. Hypothetical Thermodynamic Properties. Subcooled Vaporization Enthalpies and Vapor Pressures of Polyaromatic Hydrocarbons. *J. Chem. Eng. Data* **2008**, *53* (8), 1903−1913.
(33) Judy, C. L.; Pontikos, N. M.; Acree, W. E. Solubility of pyrene in binary solvent mixtures containing cyclohexane. *J. Chem. Eng. Data* **1987**, *32* (1), 60−62.
(34) Carvalho, S. P.; Lucas, E. F.; González, G.; Spinelli, L. S. Determining Hildebrand solubility parameter by ultraviolet spectroscopy and microcalorimetry. *J. Braz. Chem. Soc.* **2013**, *24* (12), 1998−2007.
(35) Barton, A. F. M. *Handbook of Polymer-Liquid Interaction Parameters and Solubility Parameters*; CRC Press: Boca Raton, FL, 1990.
(36) Brandrup, J.; Immergut, E. H. *Polymer Handbook*, 3rd ed.; Wiley: Hoboken, NJ, 1989.
(37) Arichi, S.; Matsuura, H.; Tanimoto, Y.; Murata, H. Studies of poly-2-vinylpyridine. ii. solubilities in various solvents. *Bull. Chem. Soc. Jpn.* **1966**, *39* (3), 434−439.
(38) Kuo, S.-W.; Lin, C.-L.; Chang, F.-C. The study of hydrogen bonding and miscibility in poly(vinylpyridines) with phenolic resin. *Polymer* **2002**, *43* (14), 3943−3949.
(39) Cui, L.; Wang, H.; Ding, Y.; Han, Y. Tunable ordered droplets induced by convection in phase-separating P2VP/PS blend film. *Polymer* **2004**, *45* (24), 8139−8146.
(40) Yu, X.; Wang, X.; Wang, H.; Li, X.; Gao, J. Prediction of solubility parameters for polymers by a QSPR model. *QSAR Comb. Sci.* **2006**, *25* (2), 156−161.
(41) Koç, D. İ.; Koç, M. L. A genetic programming-based QSPR model for predicting solubility parameters of polymers. *Chemom. Intell. Lab. Syst.* **2015**, *144*, 122−127.
(42) Schmidt, S. C.; Hillmyer, M. A. Morphological behavior of model poly(ethylene-alt-propylene)-b-polylactide diblock copolymers. *J. Polym. Sci., Part B: Polym. Phys.* **2002**, *40* (20), 2364−2376.
(43) Almdal, K.; Mortensen, K.; Ryan, A. J.; Bates, F. S. Order, Disorder, and Composition Fluctuation Effects in Low Molar Mass Hydrocarbon−Poly(dimethylsiloxane) Diblock Copolymers. *Macromolecules* **1996**, *29* (18), 5940−5947.
(44) Ndoni, S.; Papadakis, C. M.; Bates, F. S.; Almdal, K. Laboratory-scale setup for anionic polymerization under inert atmosphere. *Rev. Sci. Instrum.* **1995**, *66* (2), 1090−1095.
(45) Quirk, R. P. *Anionic Polymerization Principles and Practical Applications*; Marcel Dekker: New York, 1996.
(46) Schulz, M. F.; Khandpur, A. K.; Bates, F. S.; Almdal, K.; Mortensen, K.; Hajduk, D. A.; Gruner, S. M. Phase behavior of polystyrene−poly(2-vinylpyridine) diblock copolymers. *Macromolecules* **1996**, *29* (8), 2857−2867.
(47) Yuki, H.; Okamoto, Y.; Kuwae, Y.; Hatada, K. Stereospecific polymerization of o-methoxystyrene by anionic initiators. *J. Polym. Sci., Part A-1: Polym. Chem.* **1969**, *7* (7), 1933−1946.
(48) Hahn, S. F. An improved method for the diimide hydrogenation of butadiene and isoprene containing polymers. *J. Polym. Sci., Part A: Polym. Chem.* **1992**, *30* (3), 397−408.
(49) Bevilacqua, E. M. Degradation of Polyisoprene Networks by Oxygen. *J. Am. Chem. Soc.* **1958**, *80* (20), 5364−5367.
(50) Favre-Nicolin, V.; Cerny, R. FOX, 'free objects for crystallography': a modular approach to ab initio structure determination from powder diffraction. *J. Appl. Crystallogr.* **2002**, *35* (6), 734−743.
(51) Cheremisinoff, N. P. *Materials Selection Deskbook*, 1st ed.; Noyes Publications: Westwood, NJ, 1996.

DOI: 10.1021/acs.macromol.7b01893
Macromolecules XXXX, XXX, XXX−XXX

(52) Arichi, S.; Yoshida, M.; Ogawa, Y. The specific refractive index increment and the partial specific volume of atactic poly (2-vinylpyridine). *Bull. Chem. Soc. Jpn.* **1975**, *48* (5), 1417−1422.
(53) Choi, S.-H.; Bates, F. S.; Lodge, T. P. Structure of Poly(styrene-b-ethylene-alt-propylene) Diblock Copolymer Micelles in Squalane. *J. Phys. Chem. B* **2009**, *113* (42), 13840−13848.
(54) Wong, W.-K.; Westrum, E. F., Jr. Thermodynamics of polynuclear aromatic molecules I. Heat capacities and enthalpies of fusion of pyrene, fluoranthene, and triphenylene. *J. Chem. Thermodyn.* **1971**, *3* (1), 105−124.
(55) Jackson, C.; Chen, Y. J.; Mays, J. W. Size exclusion chromatography with multiple detectors: solution properties of linear chains of varying flexibility in tetrahydrofuran. *J. Appl. Polym. Sci.* **1996**, *61* (5), 865−874.
(56) Broughton, J. Q.; Gilmer, G. H. Thermodynamic Criteria for Grain-Boundary Melting: A Molecular-Dynamics Study. *Phys. Rev. Lett.* **1986**, *56* (25), 2692−2695.
(57) Dhar, J.; Guha, A. C. Crystal Structure of Pyrene. *Z. Kristallogr. - Cryst. Mater.* **1935**, *91*, 123−128.
(58) Camerman, A.; Trotter, J. The Crystal and Molecular Structure of Pyrene. *Acta Crystallogr.* **1965**, *18*, 636−643.
(59) Renuncio, J. A. R.; Prausnitz, J. M. An Approximation for Nonrandomness in Polymer-Solution Thermodynamics. *Macromolecules* **1976**, *9* (6), 898−903.
(60) Eitouni, H. B.; Balsara, N. P. Thermodynamics of polymer blends. In *Physical Properties of Polymers Handbook*, 2nd ed.; Springer: New York, 2007; pp 339−356.
(61) Hunter, C. A.; Lawson, K. R.; Perkins, J.; Urch, C. J. Aromatic interactions. *J. Chem. Soc., Perkin Trans. 2* **2001**, No. 5, 651−669.
(62) Desyatnyk, O.; Pszczółkowski, L.; Thorwirth, S.; Krygowski, T.; Kisiel, Z. The rotational spectra, electric dipole moments and molecular structures of anisole and benzaldehyde. *Phys. Chem. Chem. Phys.* **2005**, *7* (8), 1708−1715.
(63) Minkin, V. I. *Dipole Moments in Organic Chemistry*, 1st ed.; Plenum Press: New York, 2012.
(64) Hiemenz, P. C.; Rajagopalan, R. *Principles of Colloid and Surface Chemistry*, 3rd ed.; Marcel Dekker: New York, 1997.
(65) Shirota, Y. Photo-and electroactive amorphous molecular materials—molecular design, syntheses, reactions, properties, and applications. *J. Mater. Chem.* **2005**, *15* (1), 75−93.
(66) Müllen, K.; Scherf, U. *Organic Light Emitting Devices: Synthesis, Properties and Applications*; Wiley: Weinheim, 2006.
(67) Akbarzadeh, K.; Hammami, A.; Kharrat, A.; Zhang, D.; Allenson, S.; Creek, J.; Kabir, S.; Jamaluddin, A.; Marshall, A. G.; Rodgers, R. P. Asphaltenes—problematic but rich in potential. *Oilfield Rev.* **2007**, *19* (2), 22−43.

DOI: 10.1021/acs.macromol.7b01893
Macromolecules XXXX, XXX, XXX−XXX